(A proposal to the Jefferson Lab PAC40)

Wide-angle Compton scattering at 8 and 10 GeV photon energies

D. J. Hamilton (co-spokesperson), J.R.M. Annand, D.G. Ireland, K. Livingston, I.J.D. MacGregor, B. McKinnon, B. Seitz, D. Sokhan
University of Glasgow, Glasgow, Scotland

S. Širca (co-spokesperson), J. Beričič, M. Mihovilovič, S. Štajner
J. Stefan Institute and Dept. of Physics, University of Ljubljana, Slovenia, Slovenia

B. Wojtsekhowski (spokesperson-contact), A. Camsonne, S. Covrig, P. Degtiarenko, R. Ent, D. Gaskell, D. Higinbotham, M.K. Jones, V. Kubarovksy, P. Nadel-Turon'ski, B. Sawatzky, P. Solvignon, M. Ungaro, S.A. Wood, J. Zhang
Thomas Jefferson National Accelerator Facility, Newport News, VA 23606

I. Albayrak, M.A. Pannunzio Carmignotto, J. Denes-Couto, N. Hlavin, T. Horn, F. Klein, B. Nepal
The Catholic University of America, Washington, DC 20064

S. Abrahamyan, A. Asaturyan, A. Mkrtchyan, H. Mkrtchyan, V. Tadevosyan, A. Shahinyan, H. Voskanyan, S. Zhamkochyan
A.I. Alikhanyan National Science Laboratory, Yerevan 0036, Armenia

V. Bellini, M. Capogni, E. Cisbani, A. Del Dotto, C. Fanelli, F. Garibaldi, S. Frullani, G. Salme', G.M. Urciuoli
INFN, Italy

G.B. Franklin, V. Mamyan, B. Quinn
Carnegie Mellon University, Pittsburgh, PA 15213

R. Gilman, G. Kumbartzki, K. Myers, R. Ransome, Y. Zhang
Rutgers, The State University of New Jersey, Piscataway, NJ 08854

D. Nikolenko, I. Rachek, Yu. Shestakov
Budker Institute, Novosibirsk, Russia

W. Boeglin, P. Markowitz
Florida International University, Miami, FL 33199

V. Punjabi
Norfolk State University, Norfolk, VA 23504

B. Vlahovic
North Carolina Central University, Durham, NC 03824

T. Averrett, C. Perdrisat
College of William and Mary, Williamsburg, VA 23185

C. Hyde, A. Radyushkin, M.N.H. Rashad
Old Dominion University, Norfolk, Virginia

D. Day, R. Lindgren, D. Keller, N. Liyanage, B. E. Norum, O. Rondon
University of Virginia, Charlottesville, VA 22901
and
The Neutral Particle Spectrometer collaboration:
`https://wiki.jlab.org/cuawiki/index.php/Collaboration`

April 27, 2013

NEUTRAL PARTICLE SPECTROMETER (NPS) COLLABORATION

A. Camsonne, R. Ent, P. Nadel-Turoński, S.A. Wood, B. Wojtsekhowski
Jefferson Lab, Newport News, VA 23606

A. Asaturyan, A. Mkrtchyan, H. Mkrtchyan, V. Tadevosyan, S. Zhamkochyan
A.I. Alikhanyan National Science Laboratory, Yerevan 0036, Armenia

M. Guidal, C. Munoz Camacho, R. Paremuzyan
Institut de Physique Nucleaire d'Orsay, IN2P3, BP 1, 91406 Orsay, France

I. Albayrak, M. Carmignotto, J. Dénes-Couto, N. Hlavin, T. Horn F. Klein, B. Nepal
The Catholic University of America, Washington, DC 20064

C. Hyde
Old Dominion University, Norfolk, Virginia

P. King, J. Roche
Ohio University, Athens, OH 45701

D. Day
University of Virginia, Charlottesville, VA, USA

D. Hamilton
University of Glasgow, Glasgow, Scotland, UK

S. Sirca
University of Ljubljana, Ljubljana, Slovenia

Contents

Abstract

We propose an experiment to measure the cross-section for real Compton scattering from the proton at an incident photon energy of 8 GeV (s = 15.9 $(\mathrm{GeV}/c)^2$) and 10 GeV (s = 19.6 $(\mathrm{GeV}/c)^2$) in a broad span of scattering angles ranging from $\theta_{\mathrm{cm}} = 40^\circ$ to 120°.

The JLab RCS experiment, E99-114, demonstrated the feasibility of the experimental technique and produced remarkable results. Namely, the cross section measurement by E99-114, much more precise than the first experiment at Cornell, revealed a strong disagreement with pQCD scaling prediction in 6-GeV energy regime, but indicated that the reduced cross section could be described by a single form factor. E99-114 also observed that at s= 7 $(\mathrm{GeV}/c)^2$ and $\theta_p^{cm} = 120^\circ$, the longitudinal polarization is in agreement with the handbag description of the process in which the photons interact with a single quark, but is completely inconsistent with a pQCD mechanism which involves three active quarks interacting by two hard gluon exchanges. It is essential to have additional cross section measurements at higher photon energy over a broader kinematic range in order to identify the reaction mechanism and try to establish whether the factorization regime has been attained.

The proposed experiment utilizes an untagged bremsstrahlung photon beam and the standard cryogenic liquid hydrogen target. The scattered photon is detected in the NPS photon spectrometer, proposed for construction in Hall C. The electron beam will pass through the liquid hydrogen target. The scattered electrons will be deflected by a small magnet to allow discrimination between the elastic photon and the elastic electron scattering processes. The recoil proton will be detected in the Hall C magnetic spectrometer HMS. **With 1000 hours of beam time the precision data at highest energies will be obtained.**

Such a measurement would be of crucial importance for understanding of the reaction mechanism for this simplest process involving a real photon and it is an essential foundation for understanding of other photo-induced exclusive reactions in the JLab energy range. These RCS data will be also essential in the analysis of the two photon exchange effects in elastic electron-nucleon scattering.

1 Introduction

Compton scattering in the hard scattering limit is a powerful probe of the structure of the nucleon. Compton scattering in the wide angle regime, WACS, provides access to the high-t transverse structure of the hadron, while in the DVCS regime it provides access to the high-Q^2 low-t structure. It is a natural complement to other exclusive reactions, such as high-Q^2 elastic electron scattering and high energy meson photo-production. Two-photon coupling to the hadron allows to access the structure information which is not available from DIS and could be important in elastic electron scattering, at the same time data on the RCS process is likely more suitable for theoretical analysis than other photo reactions.

Very recently three new theoretical papers relevent for WACS were published. The calculations of two-photon effects in the soft-collinear effective theory, SCET, which has proved factorization of the handbag mechanism to the hard and soft contributions, were made by N. Kivel and M. Vanderhaeghen [1]. The SCET theory provided also a phenomenological analysis of the WACS observables. The SCET formula for the WACS cross section is very similar to the one in the handbag approach [2, 3, 4]. The GPD-based analysis of the electron-nucleon scattering form factors and WACS was updated by M. Diehl and P. Kroll with a refined prediction of the high energy WACS cross section and its form factors [5]. The formalism of the RCS theory, based on the Dyson-Shwinger Equation (DSE), have been proposed by G. Eichmann and C. Fisher [6]. The specific results for the WACS observables are not published yet. However, considering the advance of the elastic electron-nucleon form factor calculation achieved in the DSE approach [7, 8], the perspective of a microscopic theory of WACS looks very good.

For real photon Compton scattering, the hard scale is achieved when s, $-t$, and $-u$ are all large compared to the proton mass or, equivalently, when the transverse momentum transfer $p_\perp$ is large (the WACS regime). Under such conditions one expects the transition amplitude to factorize into the convolution of a perturbative hard scattering amplitude, which involves the coupling of the external photons to the active quarks, with an overlap of initial and final soft (nonperturbative) wave functions, which describes the coupling of the active quarks to the proton. Schematically this can be written as

$$T_{if}(s,t) \;\; = \;\; \Psi_f \otimes K(s,t) \otimes \Psi_i \,, \tag{1}$$

where $K(s,t)$ is the perturbative hard scattering amplitude, and the Ψ's are the soft wave functions. Different factorization schemes have been applied to RCS in recent years and these can be distinguished by the number of active constituents participating in the hard scattering subprocess. The handbag mechanism [2, 3, 4, 5] involves only one active constituent, while the perturbative QCD (pQCD) mechanism [9, 10, 11, 12, 13] involves three. In any given kinematic regime, both mechanisms will contribute, in principle, to the scattering amplitude. At "sufficiently high" energy the pQCD mechanism is expected to dominate, but it is not known how high is sufficiently high or the manner in which the transition to the purely pQCD mechanism emerges.

At relatively low energy (e.g., in the resonance region), RCS and other exclusive reactions are dominated by purely soft physics, and the amplitude does not factorize into hard and soft processes. At high energy but small $-t$ or $-u$, soft physics also dominates through Regge exchanges [28]. The nature of the transition from purely soft to the factorization regime is also not well known. Quite aside from the reaction mechanism, it is of interest to ask what RCS can teach us about the nonperturbative structure of the proton and to relate it to that revealed in other reactions.

With this backdrop, experiment E99-114 [14] was undertaken to study the RCS reaction. The primary focus was the measurement of precise spin-averaged cross sections over the kinematic regime of $5 \leq s \leq 11$ (GeV/c)^2 and $1.5 \leq -t \leq 6.5$ (GeV/c)^2. The measurement has produced the important result [15] which is shown in Fig. 1 and which will be discussed in more detail in the next section of this proposal.

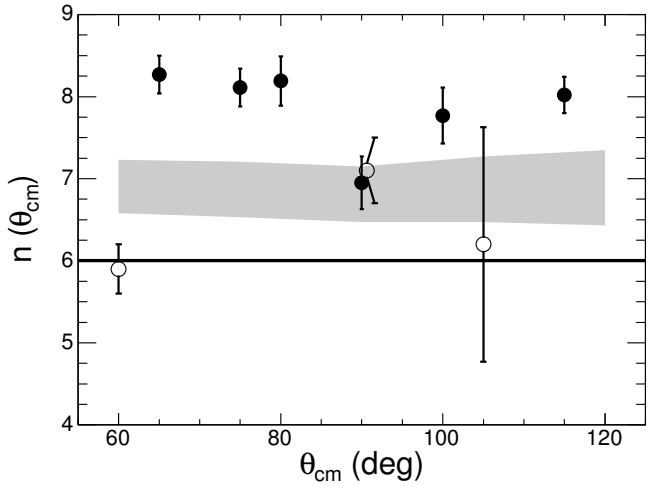

Figure 1: Scaling of the RCS cross section at fixed θ_{CM}. Full symbols denote the data from the E99-114 experiment [15]. The solid line corresponds to a constituent counting rule and scaling with fixed value $n = 6$. Open symbols denote the data from the Cornell experiment [16]. The gray band shows the range allowed by the GPD-based calculations according to [4].

In addition, a measurement was made at a single kinematic point of the polarization transfer to the recoil proton by using longitudinally polarized incident photons. The latter measurement has produced a remarkable result [17] shown in Fig. 2. Namely, the longitudinal polarization transfer is consistent with the handbag and Regge exchange predictions, while it is completely inconsistent with predictions based on pQCD. This gives very strong credence to the notion that — at least in this energy range — the photons interact with a single quark. Indeed, the longitudinal polarization is nearly as large as that expected for scattering from a free quark. However, we strongly emphasize that this is a measurement at a *single kinematic point*, and that the factorization regime might not have been reached in this case since the corresponding value of u was only -1.1 (GeV/c)^2.

This result is so intriguing that it is essential to verify E99-114 findings with measurements over a broader kinematic range, especially for higher photon energies. At 8 and 10 GeV photon energy the factorization condition that all kinematical variables are much larger than the proton mass is unequivocally met.

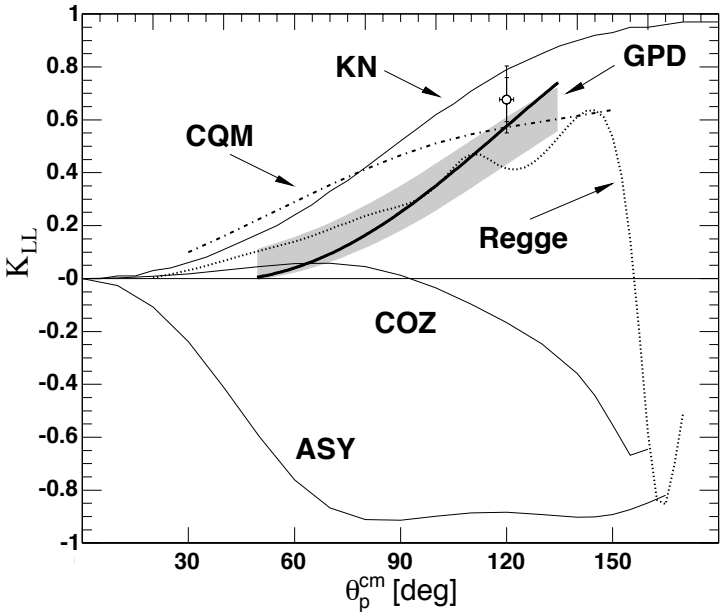

Figure 2: Longitudinal polarization transfer in the RCS process at an incident energy of 3.23 GeV [17]. The labels on the curves are KN for the asymmetry in the hard subprocess; GPD, shown as a gray band, for the handbag approach using GPD's [18]; CQM for the handbag approach using constituent quarks [19]; Regge for a Regge exchange mechanism [20]; and COZ and ASY for pQCD calculations [12] using the asymptotic (ASY) or Chernyak-Ogloblin-Zhitnitsky (COZ) distribution amplitudes.

We propose new measurements of the differential cross section in Compton scattering at incident energies of 8 and 10 GeV, or $s = 15.9$ and 19.6 $(\mathrm{GeV}/c)^2$ in a broad span of scattering angles ranging from $\theta_{\mathrm{cm}} = 40^\circ$ to 120°. These will be first measurements ever to investigate WACS at photon energies above 6 GeV. The range of the variable t will be almost double compared to the previous experiment [14]. As the values of s, $-t$ and $-u$ will all be large, the experiment will provide a much firmer grip on the way factorization is realized. Even if this answer remains elusive, the experiment will provide unique data for testing QCD based theories and an important input for the two-photon exchange calculations and GPD models.

The proposal is organized as follows. In Section 2 we present our physics motivation and summarize the physics goals of the proposed experiment. In Section 3 we describe the experimental approach and both the standard and the specialized equipment. In subsequent sections, we present our proposed measurements , our expected results and beam time request (Sec. 4), and the technical considerations related to the equipment construction and the experiment schedule (Sec. 5). The proposal is summarized in Section 6.

2 Physics Motivation

In view of the remarks in the Introduction, we consider several interesting questions that motivate us to explore further the cross section measurement in WACS at JLab:

1. Is it indeed true that the RCS reaction proceeds through the interaction of the photons with a single quark?
2. What information can be obtained about the structure of the proton from new measurements of the WACS form factor $R(t)$?
3. At what kinematic scale is pQCD scaling beginning to work?

We next present briefly the discussions of WACS in the pQCD limit, the soft-collinear effective theory, the handbag approach with GPDs, the DSE development for WACS, and the relativistic constituent quark model.

2.1 pQCD Mechanism

The traditional framework for the interpretation of hard exclusive reactions has been perturbative QCD (pQCD) [21]. This is based in part on the observation that the onset of scaling in Deep Inelastic Scattering (DIS) occurs at the relatively low scale of $Q^2 \sim 1$–2 $(\mathrm{GeV/c})^2$, thereby giving rise to expectations that pQCD might also be applicable to the exclusive processes in the range of a few $(\mathrm{GeV}/c)^2$. The pQCD approach to RCS [9, 10, 11, 12, 13] is shown in Fig. 3, where it is seen that all three valence quarks are active participants in the hard subprocess, which is effected by the exchange of two hard gluons, while the soft physics is contained in the valence quark distribution amplitudes.

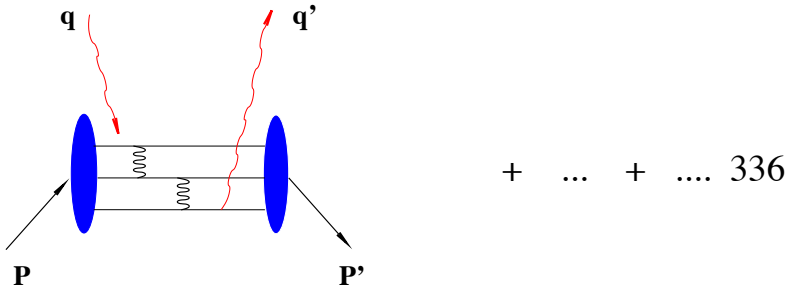

Figure 3: Two gluon exchange pQCD diagram (plus about 336 similar) for RCS.

The pQCD mechanism leads naturally to the so-called constituent counting rules for exclusive processes:

$$\frac{d\sigma}{dt} = \frac{f(\theta_{cm})}{s^n}, \tag{2}$$

where n is related to the number of active constituents in the reaction [22, 23]. Indeed, the observation that many exclusive reactions, such as elastic electron scattering, pion photoproduction, and RCS, approximately obey Eq.2 has led to the belief that the pQCD mechanism dominates at experimentally accessible energies. There seems to be little theoretical disagreement that the pQCD mechanism dominates at sufficiently high energies [24]; however, there is no consensus on how high is "sufficiently high." Indeed, despite the observed scaling, absolute cross sections calculated using the pQCD framework are very often low compared to existing experimental data, sometimes by more than an order of magnitude. Moreover, several recent JLab experiments that measure polarization observables also disagree with the predictions of pQCD. In the G_E^p experiment [25, 26] the slow falloff of the Pauli form factor $F_2(Q^2)$ up to Q^2 of 5.5 $(\mathrm{GeV}/c)^2$ provides direct evidence that hadron helicity is not conserved, contrary to predictions of pQCD. Finally, in the recently completed RCS experiment, E99-114, the preliminary analysis of the longitudinal polarization transfer K_{LL} (which will be defined precisely below) shows a value which is large and positive, contrary to the pQCD prediction which is negative. Moreover, the E99-114 data are consistent with a scaling factor $n \approx 7.5 - 8$ rather than the value $n = 6$, which is expected from pQCD and was consistent with earlier, less precise data [16] (see Fig. 1).

A recalculation of the pQCD mechanism and reassessment in light of the E99-114 data has recently been completed by Thompson et al. [13]. It is argued in this work that K_{LL} should be measured in a regime where the kinematical variables are all significantly larger than the proton mass scale, which was not the case in E99-114. They further argue that the observed decrease in the scaled cross section as s increases is consistent with a view that the onset of the asymptotic regime will soon be accessible. Moreover, some commonality between the pQCD and handbag mechanisms has been indicated, with the suggestion that inclusion of higher twist effects will introduce the necessary proton helicity flip contributions in order to better account for available data.

The differences and similarities between the precision experimental data for these reactions and the pQCD predictions mentioned above (see, for example, the recent analysis [27]) suggest a very intriguing question about the origin of the observed scaling at experimentally accessible energies, and also:

— why the cross section $d\sigma/dt$ scales as s^{-n}, and

— why the experimental power parameter n is close to the pQCD prediction?

Careful investigation of the WACS process could be a productive way to discover the answers.

2.2 Two-photon physics in SCET

The soft-collinear effective theory, SCET, was developed for electron-proton scattering at large momentum transfer [1]. The QCD factorization approach formulated in the framework of SCET allowed one to develop a description of the soft-spectator scattering contribution. The two-photon exchange (TPE) corrections were calculated in the region where the kinematical variables describing the elastic electron-proton scattering are moderately large relative to

the soft hadronic scales (M_p and Λ_{QCD}). This calculation includes the two-photon exchange contributions, TPE, to the scattering amplitude and factorizes these with a SCET form factor $\mathcal{F}_1(Q)$. The same form factor also naturally arises in wide-angle Compton scattering.

The unpolarized cross section describing Compton scattering has the form:

$$\frac{d\sigma}{dt} \simeq \frac{2\pi\alpha^2}{(s-m^2)^2}\left(\frac{1}{1-t/s}+1-t/s\right)|\mathcal{R}|^2 = \frac{d\sigma^{KN}}{dt}|\mathcal{R}|^2, \tag{3}$$

where $d\sigma^{KN}$ is the Klein-Nishina cross section corresponding to a point-like massless particle.

The values $|\mathcal{R}^{exp}| = \sqrt{d\sigma^{exp}(s,t)/d\sigma^{KN}(s,t)}$ extracted from the data [15] are shown in Fig. 4 showing the results at three different values of the invariant mass: $s = 6.8$, 8.9 and 10.9 GeV^2 at $2.5 < -t < 6.5$ GeV^2. As one can see from this plot, the extracted values $|\mathcal{R}^{exp}|$ do not show any significant dependence on the values of s, as required by factorization. However, in the large range of t the measurements are performed only at one value of s. It would be of large interest to find how this prediction works at much higher values of s over the same range of t (as it is proposed in this experiment).

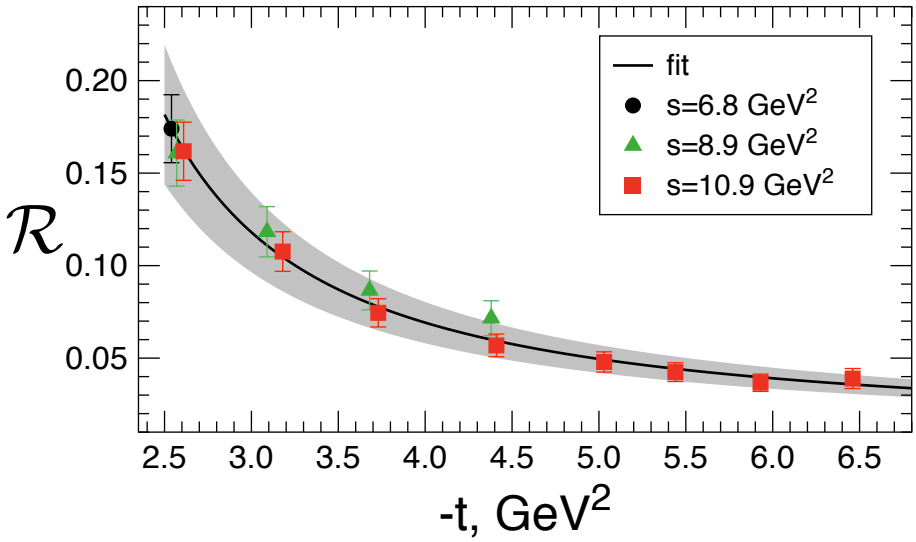

Figure 4: The ratio $\mathcal{R}$ extracted from the WACS data [15] and the fit [1] without kinematic power corrections. The gray band shows the 1σ error bands.

2.3 Handbag Mechanism and GPD-based Models

The handbag mechanism offers new possibilities for the interpretation of hard exclusive reactions. For example, it provides the framework for the interpretation of so-called deep exclusive reactions, which are reactions initiated by a high-Q^2 virtual photon. The application of the formalism to RCS (see Fig. 5) was initially worked out to leading order (LO) by A. Radyushkin [2] and subsequently by M. Diehl and collaborators [3]. More recently

next-to-leading-order (NLO) contributions have been calculated by H. Huang and P. Kroll [4].

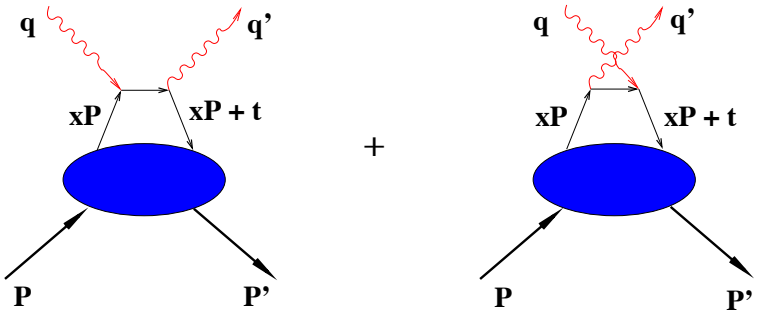

Figure 5: The handbag diagram (left) and the crossed term (right) for RCS.

The corresponding diagram for elastic electron scattering is similar to Fig. 5, except that there is only one external virtual photon instead of two real photons. In the handbag approach, the hard physics is contained in the scattering from a single active quark and is calculable using pQCD and QED: it is just Compton scattering from a structureless spin-1/2 particle.

The soft physics is contained in the wave function describing how the active quark couples to the proton. This coupling is described in terms of GPD's.

The GPD's have been the subject of intense experimental and theoretical activity in recent years since the original articles [29, 30]. They represent "superstructures" of the proton, from which other measurable structure functions are derived, such as parton distribution functions (PDF) and form factors. To NLO, only three of the four GPD's contribute to the RCS process: $H(x,\xi=0,t)$, $\hat{H}(x,\xi=0,t)$, and $E(x,\xi=0,t)$. Since the photons are both real, the so-called skewness parameter ξ=0, reflecting the fact that the momentum absorbed by the struck quark is purely transverse.

In the handbag formalism, the RCS observables are new form factors of the proton that are x^{-1}-moments of the GPD's:

$$
\begin{aligned}
R_{_V}(t) &= \sum_a e_a^2 \int_{-1}^{1} \frac{dx}{x} H^a(x,0,t), \\
R_{_A}(t) &= \sum_a e_a^2 \int_{-1}^{1} \frac{dx}{x}\, sign(x)\, \hat{H}^a(x,0,t), \\
R_{_T}(t) &= \sum_a e_a^2 \int_{-1}^{1} \frac{dx}{x} E^a(x,0,t),
\end{aligned}
$$

where e_a is the charge of the active quark and the three form factors are, respectively, the vector, axial vector, and tensor form factors. The corresponding form factors for elastic

electron or neutrino scattering are given by the x^0-moments of the same GPD's:

$$\begin{aligned} F_{_1}(t) &= \sum_a e_a \int_{-1}^{1} dx\, H^a(x,0,t), \\ G_{_A}(t) &= \sum_a \int_{-1}^{1} dx\, sign(x)\, \hat{H}^a(x,0,t), \\ F_{_2}(t) &= \sum_a e_a \int_{-1}^{1} dx\, E^a(x,0,t), \end{aligned}$$

where the three quantities are, respectively, the Dirac, axial, and Pauli form factors. On the other hand, the $t = 0$ limit of the GPD's produce the PDF's:

$$\begin{aligned} H^a(x,0,0) &= q^a(x), \\ \hat{H}^a(x,0,0) &= \Delta q^a(x), \\ E^a(x,0,0) &= 2\frac{J^a(x)}{x} - q^a(x), \end{aligned} \tag{4}$$

where J^a is the total angular momentum of quark flavor a and is not directly measurable in DIS.

In the handbag factorization scheme, the RCS helicity amplitudes are related to the form factors by

$$\begin{aligned} M_{\mu'+,\mu+}(s,t) &= 2\pi\alpha_{em}\left[T_{\mu'+,\mu+}(s,t)(R_{_V}(t)+R_{_A}(t)) + T_{\mu'-,\mu-}(s,t)(R_{_V}(t)-R_{_A}(t))\right], \\ M_{\mu'-,\mu+}(s,t) &= 2\pi\alpha_{em}\frac{\sqrt{-t}}{m}\left[T_{\mu'+,\mu+}(s,t) + T_{\mu'-,\mu-}(s,t)\right] R_{_T}(t), \end{aligned}$$

where μ, μ' denote the helicity of the incoming and outgoing photons, respectively. The signs on indices of M and T refer to the helicities of the proton and the active quark, respectively. This structure of the helicity amplitudes leads to a simple interpretation of the RCS form factors: $R_{_V} \pm R_{_A}$ describe the response of the proton to the emission and re-absorption of quarks with helicity in the same/opposite direction with respect to the proton helicity, and $R_{_T}$ is directly related to the proton helicity-flip amplitude [4].

These equations lead to expressions relating RCS observables to the form factors. The most important of these experimentally are the spin-averaged cross section and the recoil polarization observables. The spin-averaged cross section factorizes into a simple product of the Klein-Nishina (KN) cross section describing the hard scattering from a single quark and a sum of form factors depending only on t [2, 3]:

$$\frac{d\sigma/dt}{d\sigma_{_{\rm KN}}/dt} = f_{_V}\left[R_{_V}^2(t) + \frac{-t}{4m^2}R_{_T}^2(t)\right] + (1-f_{_V})R_{_A}^2(t)\,. \tag{5}$$

For the the interesting region of large $p_\perp$, the kinematic factor $f_{_V}$ is always close to 1. Consequently the unpolarized cross sections are largely insensitive to $R_{_A}$, and the left-hand-side of Eq. (5) is nearly s-independent at fixed t. The recent calculations to NLO, which take

into account both photon and proton helicity-flip amplitudes, do not change this prediction in any appreciable way [4]. A new analysis of the GPDs recently performed by Diehl and Kroll [5], gave an updated prediction for the WACS cross section, see Fig. 6.

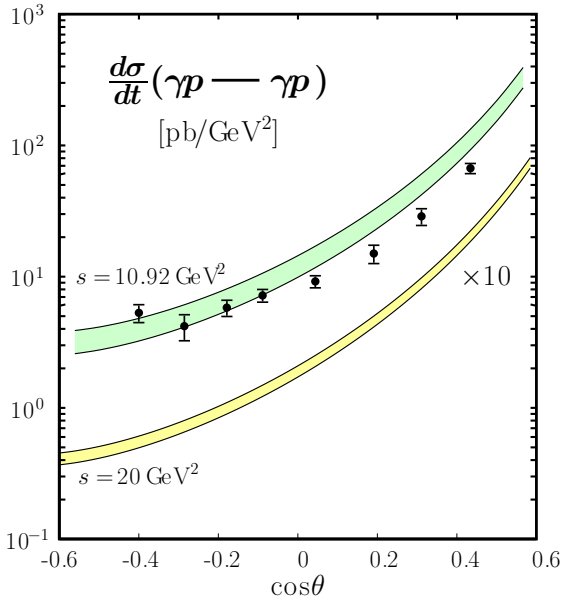

Figure 6: The GPD-based prediction for the WACS cross section [5].

2.4 Real Compton Scattering in the DSE approach

For all the insight that we gain from pQCD, we learn rather little about many of the most important issues concerning nucleon structure , such as the dynamical generation of mass through Dynamical Chiral Symmetry Breaking (DCSB), or quark confinement. There are, however, analytical techniques that at least in principle appear to have the potential to provide solutions to QCD in the non-perturbative regime with arbitrarily high accuracy. One such technique is based on the infinite tower of Dyson-Schwinger equations (DSEs) that relate the Green's functions of a field theory to each other [33]. In principle, solving the DSE's provides a solution to any field theory. In any practical calculation, however, the DSEs must be truncated, and some Ansätze must be employed to account for the omitted functions. By carefully maintaining certain properties of the theory, however, such as local and global symmetries, considerable progress can be made. Recent calculations, for instance, explicitly describe the dynamic generation of the mass of constituent quarks, and show excellent agreement with the lattice QCD results that necessarily assume large current-quark masses. In Fig. 7 the dressed-quark mass function $M(p)$ is shown as a function of momentum for each of three bare-quark masses.

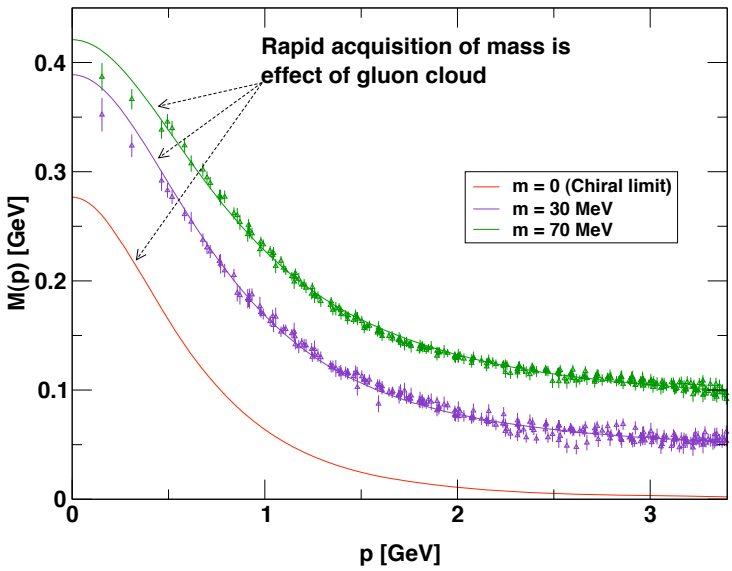

Figure 7: Dressed-quark mass function, $M(p)$. The solid curves show DSE results and the "data" represent unquenched LQCD calculations. In this figure one observes the current-quark of perturbative QCD evolving into a constituent-quark as its momentum becomes smaller.

Using dressed quarks as the elementary degrees of freedom, one can calculate nucleon form factors using a Poincaré covariant Faddeev equation, as has been done recently by C. D. Roberts and collaborators [7, 8]. These authors also assume that two of the quarks couple into a diquark. While still an approximation, the DSE/Faddeev approach is in part based on first principles. It is limited, however, in that there are precisely three (and for instance, not five) constituent quarks used as an input to the calculation. Even so, as mentioned earlier, it is reasonable to assume the dominance of the three-quark component of the wave function at relatively high values of Q^2. The DSE/Faddeev calculations provide a remarkably good description of the available elastic electron-nucleon form factor data, which is likely telling us a fairly profound fact about the nucleon's structure.

These advances of the form factors calculations lead to expectation that the WACS process could be also calcuated in the DSE approach. Indeed, in the recent paper [6] the relevant phenomenology of the RCS has been developed. However, the calculations for specific observables are not avaible yet.

2.5 Handbag Mechanism in a Relativistic Constituent Quark Model

A different formulation for RCS in the handbag approach that differs significantly from the GPD formalism described above is that of Miller [19]. In his approach the handbag diagram involves γq scattering, as before, and proton wave functions obtained from relativistic Constituent Quark Models (CQM). What distinguishes this approach from both the Lead-

ing Order GPD and pQCD models is the fact that these proton wave functions explicitly include the influence of quark transverse momenta and configurations involving non-zero quark orbital angular momentum. This naturally corresponds to violation of proton helicity conservation. Indeed, non-conservation of proton helicity in this model has proven to be one of the key factors in its successful account of electromagnetic form factor data for the proton [31, 32].

The calculations for RCS involve evaluating the handbag diagrams of Fig. 5 in an impulse approximation. The resulting reaction amplitude depends on proton wave functions obtained from Poincaré invariant calculations involving constituent quark models in light-front dynamics. These wave functions have previously been constrained by proton electromagnetic form factor data in the same kinematic regime [32]. Significant contributions to the wave functions from quark transverse momenta and orbital angular momentum are natural feature of the relativistic calculations.

Reasonable agreement with RCS cross section data has been obtained with a slight modification of the constituent quark masses [19]. In the case of the RCS spin observables, a similar large value of K_{LL} as for the GPD approach (see Fig.2), and a value for the transverse polarization transfer of $K_{LT}= 0$ have been predicted.

2.6 Summary of Physics Goals

We propose measurements of the cross-section for real Compton scattering at an incident photon energy of 8 GeV ($s = 15.9$ (GeV/c)^2) and 10 GeV ($s = 19.6$ (GeV/c)^2) in a broad span of scattering angles ranging from $\theta_{\rm cm} = 40^\circ$ to 120°. The specific physics goals are as follows:

1. Provide first determination of the WACS cross section at photon energies 8 and 10 GeV, which is significantly above previous experiments, almost doubling the range of t.
2. Measure the cross section scaling parameter at fixed θ_{cm} for s up to 19.6 (GeV/c)^2.
3. Measure the WACS from factor and test predictions of the SCET- and GPD-based calculations.

The overall statistical precision with which we will address these physics goals will be discussed in Sec. 4.

3 Experimental Setup

The configuration of the experimental setup is similar to the one used in the E99-114 (Hall A RCS [14]) and in the E07-002 (Hall C RCS [34]) experiments. The recoiled protons will be detected in the High-Momentum Spectrometer (HMS) in standard configuration. The Compton-scattered photons will be detected by the Neutral Particle Spectrometer (see Figs. 8 and 9) which, along with other key equipment, is described in the following.

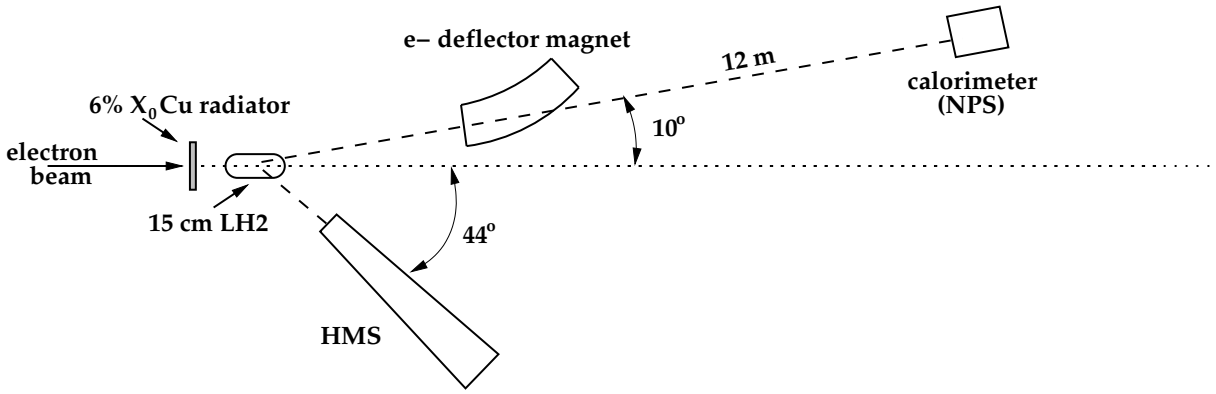

Figure 8: Schematic of the setup 5A at 10 GeV with HMS detecting the recoiled protons and the photon calorimeter detecting the Compton-scattered photons in addition to a fraction of elastically scattered electrons which will be partly removed by the deflector magnet. The magnet will in fact be vertically bending for reasons outlined below.

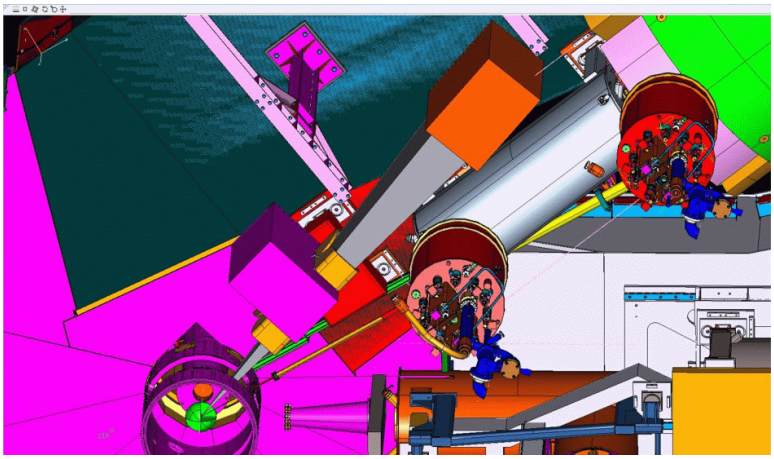

Figure 9: Proposed setup of the WACS experiment in Hall C. Looking downstream from the scattering chamber the deflection magnet, the helium bag and the calorimeter frame can be seen. The calorimeter in this configuration is located beam-left relative to the beam-pipe and on the left side of the SHMS spectrometer.

3.1 The CEBAF electron beam

Based on our experience with E99-114, we opt for an incident unpolarized electron beam with a current of 60 μA delivered in Hall C. Combined with the 10 cm long LH2 target this implies an average luminosity of $\mathcal{L}_{\rm ep} = 1.58 \cdot 10^{38}/{\rm Hz/cm^2}$.

3.2 The High-Momentum Spectrometer

The recoiled protons in the proposed experiment will be detected by the High-Momentum Spectrometer (HMS), which is part of the standard equipment of Hall C. The HMS is a high-resolution ($\delta p/p < 10^{-3}$) magnetic spectrometer in a QQQD magnet configuration with a maximum momentum of 7.5 GeV/c and a momentum bite of 18 %. It has an octagonal input aperture with an effective solid angle coverage of approximately 6 msr and can be positioned to angles greater than 12.5°.

The HMS can be tuned in parallel-to-point mode (for optimal in-plane angle accuracy) or point-to-point mode (for best vertex reconstruction). In the proposed experiment it will be used in the latter mode in which extended targets can be accommodated with a vertex reconstruction accuracy of ≈ 1 mm, and where both in-plane and out-of-plane angle measurement precisions are about 0.8 mrad.

The detector package of the HMS consists of two vertical drift chamber packages for track reconstruction, scintillator hodoscopes for timing, as well as a gas Čerenkov counter, an aerogel Čerenkov counter, and a segmented lead-glass shower calorimeter for particle identification. If needed, the shower calorimeter will be used in the trigger.

3.3 The Liquid Hydrogen Target and the Radiator

The experiment will utilize one of the standard Hall C liquid hydrogen (LH2) targets with a 10 cm-long machined cell with aluminum walls of 5 mil thickness, which was successfully employed in many experiments in JLab. The copper radiator with a thickness of $t_{\rm rad}/X_0 = 0.06$ (6 % of radiation length) will be mounted on the cell block about 4 inches upstream of the cell entrance window. The short distance between the target and the radiator helps avoid background produced the walls of the target and keep the photon beam spot compact, which allows accurate measurement of the proton momentum with vertical bend spectrometer and operation with high luminosity. Note that in the rate simulations, the effective thickness of the radiator was assumed to be slightly larger, $t_{\rm rad}/X_0 = 0.08$, due to additional radiative processes in the target and the virtual photon flux.

3.4 Deflection magnet

It was shown in the E99-114 experiment that the deflection magnet provides an effective way to discriminate between electron and photon elastic scattering events. The magnet obviates the need for a veto detector, which in turn allows us to utilize at least ten times higher

photon/electron beam intensity. The design of the magnet has been driven by a number of considerations:

- Aperture for the full size of the calorimeter;
- Magnetic field for electron deflection;
- Minimum magnetic field at the beam line;
- Horizontal orientation of the magnetic field.

Additional information about the magnet design is presented in the Sec. 5.

3.4.1 Choosing the bending direction

One of the key aspects in online and offline discrimination of real-Compton from background events is a reliable comparison of the expected and actually measured electron-proton (calorimeter-HMS) correlation. The *angular spread* of this correlation is smaller out-of-plane because it is defined only by angular resolution; in contrast, it is larger in-plane because its dominant contribution comes from the HMS momentum resolution, which relative value is $\delta p/p \approx 10^{-3}$. Typically the out-of-plane resolution relevant for the e-p correlation is twice as good as the in-plane resolution. The bending direction for elastic electrons should therefore be vertical (magnetic field horizontal) in order to minimize required deflection of electrons and resulting value of the field in the deflection magnet.

3.4.2 Determining the required field integral

The energies of the proposed experiment are about twice as large as those encountered in E99-114, with the consequence that the angular distribution (and the corresponding spatial distribution at some drift distance) of decay photons from photo-produced π^0 will be rather focused, resulting in a real-Compton peak superimposed on a relatively narrow distribution of π^0 decay photons. As result the pion related contribution in the final event sample will reach about 17 for the $\pm 3\sigma$ cut (see Tables 1 and 2 below). This means that the shape of the pion related events need to be well understood. The role of the deflector magnet is therefore not only to separate the elastic electrons from real-Compton photons, but also to relocate the electrons sufficiently far from the $\pi^0 \rightarrow 2\gamma$ events. This can be accomplished by a sufficiently strong deflector magnet. A magnet that will be able to provide a field integral of up to $\int \vec{B} \cdot \mathrm{d}\vec{l} \approx 0.6\,\mathrm{Tm}$ has been designed and will be constructed for the proposed experiment. It will be placed as indicated in Fig. 9 which shows a typical setup.

3.5 The photon calorimeter

This experiment is possible due to construction of the new facility: a Neutral Particle Spectrometer [37]. This photon calorimeter will consist of a rectangular array of 1116 =

31 (hor) $\times$ 36 (vert) $PbWO_4$ crystal blocks with dimensions $2.05 \times 2.05 \times 18\,\mathrm{cm}^3$ with their associated PMTs and high-voltage (HV) dividers, as well as the corresponding mechanical and electronics systems. Figure 10 shows the array of crystal blocks that will closely resemble the one that will be used in the proposed experiment, and is based on the HYCAL [38] detector.

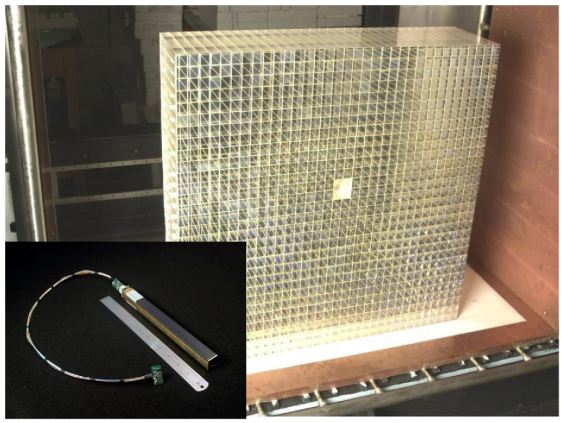

Figure 10: The high-resolution $PbWO_4$ part of the HYCAL detector on which the present calorimeter design is based.

The PMTs are shielded from ambient light in a light-tight box that contains an air-cooling system, whose main purpose is to prevent the PMTs from overheating and aid in the overall stable operation of the calorimeter: the yield of the $PbWO_4$ crystals is temperature-dependent, with $\approx -2\,\%/^\circ\mathrm{C}$ deterioration of light yield around room temperature. HV and signal-cable systems are also contained in the light box encasing the PMTs.

The calorimeter will be equipped with a system that distributes light pulses to each calorimeter module. The main purpose of this system is to provide a quick way to check the detector operation and to calibrate the dependence of the signal amplitudes on the applied HV. The detector response to photons of a given energy may drift with time, due to drifts in the PMT gains and to changes in the glass transparency caused by radiation damage. For this reason, the gain monitoring system will also allow measurements of the relative gains of all detector channels during the experiment.

The calorimeter can be moved into the hall without being disconnected from the front-end electronics which is located in racks a few feet behind the main detector components. The position of the photon arm will be adjusted for each kinematics to match the angular position of the HMS. The calorimeter will most likely be placed on rails and repositioned by sliding along these rails. In previous experiments less than two hours' time (beam-off to beam-on) were required to move the calorimeter in a typical hall access.

Due to radiation issues (see below) it will be very beneficial to place a 10 cm thick plastic cover with an effective surface area thickness of approximately $10\,\mathrm{g/cm}^2$ in front of the calorimeter. This is in agreement with experience from E99-114.

3.5.1 Trigger of the DAQ

In contrast to E99-114, where a particular coincidence trigger scheme was used, *we will use only the HMS trigger* in this experiment. This is possible because the new HMS and NPS electronics has practically zero dead time, so each particle detected by the HMS will trigger the DAQ readout of both the HMS and the calorimeter. The cluster summing described [17] will therefore not be implemented in the trigger, as it was the case in E99-114. However the standard shower analysis will be performed offline.

3.6 Monte-Carlo simulation of the experimental setup

The details of the experimental setup have been studied by a GEANT4-based Monte-Carlo simulation tool developed at University of Glasgow [39]. The focus was on estimating the counting rates, backgrounds and resolutions (shown in Tables 1 and 2).

The mixed electron-photon beam has been simulated by incorporating electro-magnetic processes in the radiator and target in order to generate realistic energy and angular distributions of photon and electron beams. The simulations were performed with both beam energies (8.8 and 11 GeV) for the 6 % radiation length radiator and 10 cm LH2 target.

The simulation of the photon arm included the target cell by taking into account its geometry and all materials, the scattering chamber, the deflection magnet and the calorimeter. The deflection magnet has been placed at distances of 1.1 to 2.45 m from the target; as mentioned previously, vertical bending has been used that is crucial for the separation of real-Compton and e-p elastic events. The calorimeter has been implemented as a virtual detector with front-face dimension of 64 cm × 74 cm and a depth of 18 cm, positioned at various distances from the target, depending on the kinematic setting. The 10 cm plastic shielding has also been incorporated. In our simulations we have assumed for the calorimeter coordinate resolution a typical value of 3 mm, and energy resolution of $0.023{\cdot}\sqrt{E(\mathrm{GeV})}$.

The proton tracks from the event generator are fed into a SIMC simulation that performs a multiple scattering calculation before tracking the protons through the HMS optics, determining whether it is within the acceptance and outputting reconstructed proton kinematic variables at the target ($\delta, dx/dz, dy/dz$ and y_{tgt}). In this instance, the HMS is simulated with an open collimator. This output is then merged and synchnonized with the Geant4 output for analysis of the two-arm simulated data within ROOT.

3.6.1 Calorimeter occupancy and energy resolution

At high luminosities anticipated in the proposed experiment there is a large probability of two or more high energy events within the time resolution of the photon detector. We obtained that probability as a function of the detection threshold from the MC above as well as from previous RCS measurements.

Table 3 shows the probability of a second hit with energy above 0.25 and 0.50 of the WACS photon energy for the five-path kinematics.

Table 1: Parameters and results for the GEANT4 simulation of kinematics 4A—4G. They are the incident photon energy, E_{in}, the photon scattering angle for the center of the calorimeter, θ_γ, the energy of scattered photon, E_γ, the angle of the recoil proton, θ_p, the momentum of the recoil proton, p_p, the distance from the target to the calorimeter front, D_{calo}, the distance from the target to the magnet center, D_{magnet}, the field integral used in MC, $\int B.dl$, the deflection of the electron hit at the calorimeter front, Δ_{e^-}, the resolution of the horizontal difference between the observed and expected hit coordinate at the calorimeter, σ_x, the same for vertical difference, σ_y.

	4A	**4B**	**4C**	**4D**	**4E**	**4F**	**4G**
E_{in} [GeV]	8.0	8.0	8.0	8.0	8.0	8.0	8.0
θ_γ [°]	11	15	19	28	33	40	48
E_γ [GeV]	6.917	6.199	5.463	4.004	3.368	2.671	2.094
θ_p [°]	47.47	38.57	32.10	22.83	19.51	16.09	13.27
p_p [GeV/c]	1.791	2.574	3.347	4.844	5.491	6.196	6.780
D_{calo} [m]	11.0	9.0	6.0	3.5	3.0	2.5	2.5
D_{magnet} [m]	2.45	2.45	1.65	1.1	1.1	1.1	1.1
$\int B.dl$ [Tm]	0.25	0.3	0.35	0.6	0.6	0.6	0.6
Δ_{e^-} defl [cm]	9.12	9.18	7.93	9.50	8.54	7.28	7.97
σ_x [cm]	5.35	3.86	2.41	1.42	1.29	1.15	1.32
σ_y [cm]	1.07	1.05	0.84	0.81	0.86	0.98	1.11

3.6.2 Calorimeter drift distance optimization

It would appear natural to position the calorimeter as closely as possible to the target in order to maximize the angular acceptance and therefore the rate of real-Compton events (see Fig. 11). But placing it too far also amounts to truncating the distribution of $\pi^0 \to 2\gamma$ events, thus jeopardizing the control of systematics. The drift distances listed in Tables 1 and 2 have therefore been optimized with this trade-off in mind.

Table 2: Parameters for the GEANT4 simulation of kinematics 5A—5F. The notations are the same as in Table 1.

	5A	**5B**	**5C**	**5D**	**5E**	**5F**
E_{in} [GeV]	10.0	10.0	10.0	10.0	10.0	10.0
θ_γ [°]	10	14	18	24	30	36
E_γ [GeV]	8.607	7.596	6.572	5.205	4.119	3.295
θ_p [°]	44.44	34.94	28.44	21.98	17.75	14.79
p_p [GeV/c]	2.135	3.208	4.264	5.656	6.754	7.586
D_{calo} [m]	12.0	9.0	7.0	4.5	3.25	2.75
D_{magnet} [m]	2.45	2.45	1.65	1.65	1.1	1.1
$\int B.dl$ [Tm]	0.25	0.35	0.4	0.5	0.6	0.6
e^- defl [cm]	8.20	8.76	9.24	7.48	8.10	7.25
σ_x [cm]	5.85	3.29	2.42	1.65	1.33	1.27
σ_y [cm]	0.82	0.91	0.94	0.89	0.85	0.98

Table 3: Rates for kinematics 5A—5F at beam current of 60 μA and conditions per Table 2.

	5A	**5B**	**5C**	**5D**	**5E**	**5F**
HMS proton rate, Hz	1400	68	21	7	6	5
HMS pion rate, Hz	0.5	1	2	4	5	5
NPS rate ($E > 0.5E_{RCS}$), Hz	934	42	16	13	16	14
NPS rate ($E > 0.2E_{RCS}$), Hz	2975	130	52	35	39	34
RCS rate, per hour	900	220	85	40	25	15
Beam time for 10% accuracy, hour	3	11	29	63	100	167

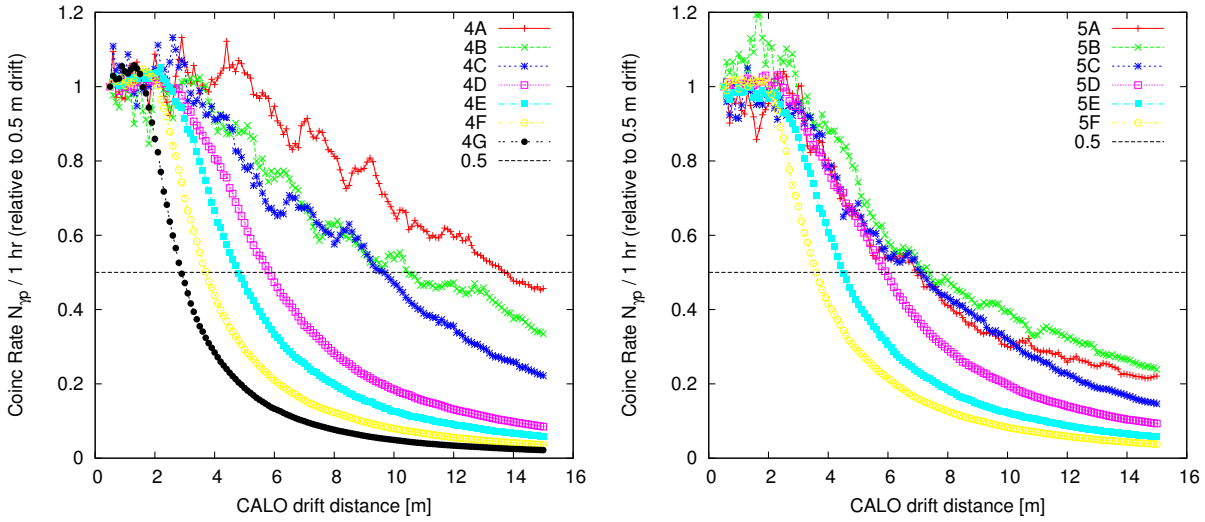

Figure 11: The simulated rate of γ-p (real-Compton) coincidences as a function of calorimeter drift distance (normalized to rate at 0.5 m drift) for kinematics 4A—4G ($E_\gamma = 8\,\mathrm{GeV}$). [RIGHT] Same for kinematics 5A—5F ($E_\gamma = 10\,\mathrm{GeV}$). The horizontal line denotes the relative decrease in the coincidence rate by a factor of two. The apparent rate increase with increasing calorimeter distance is caused by noise (low statistics) in MC data.

4 Expected Results and Beam Time Request

4.1 Expected Results

To extrapolate the E99-114 data to higher s and $-t$, we have used the formula

$$\frac{\mathrm{d}\sigma}{\mathrm{d}t}(s,t) = 0.0702 \left(\frac{s_0}{s}\right)^2 \left(\frac{t_0}{t}\right)^4 \left[\frac{\mathrm{nb}}{\mathrm{GeV}^2}\right] , \quad s_0 = 10.92\,\mathrm{GeV}^2 , \quad -t_0 = 2.61\,\mathrm{GeV}^2 . \qquad (6)$$

We expect a combined statistical and systematic uncertainty of 10 %. The expected results for the total beam time of 1000 hours (including overhead for all setup changes) with 450 h spent in kinematics 4A—4G ($s = 15.9\,\mathrm{GeV}^2$) and 550 h in kinematics 5A—5F ($s = 19.6\,\mathrm{GeV}^2$) are shown in Fig. 12.

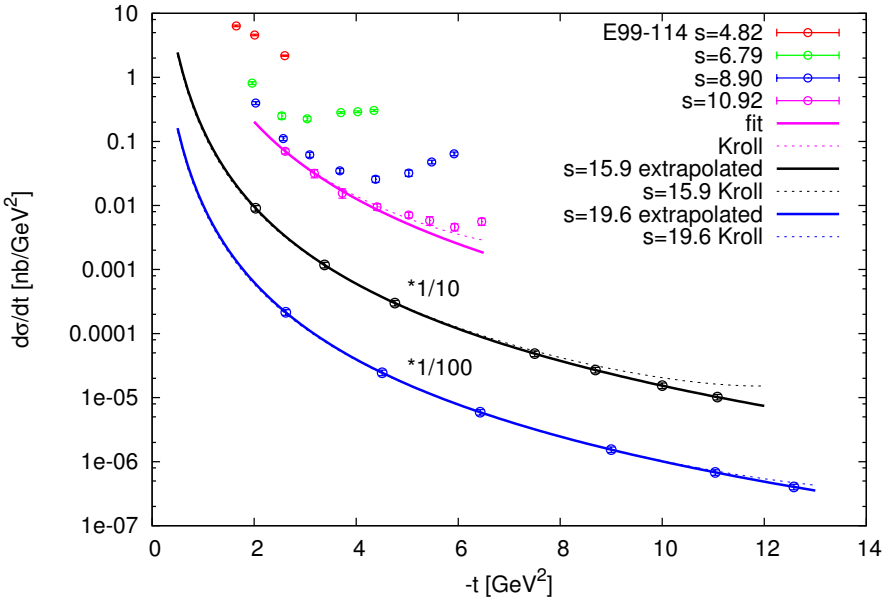

Figure 12: The anticipated data points of the proposed experiment at $s = 15.9\,\mathrm{GeV}^2$ (black symbols) and at $s = 19.6\,\mathrm{GeV}^2$ (blue symbols), together with the existing cross-sections from E99-114 [15], for the total beam time of 1000 hours. The expected points are drawn on the curves (black and blue) obtained by extrapolating the E99-114 cross-sections according to (6), which differ from the recent prediction by Diehl and Kroll [5] only at large t. The error bars are combined statistical and systematic.

5 Technical Considerations

The key new element of instrumentation in this experiment is a photon calorimeter - Neutral Particle Spectrometer, which is proposed for construction in Hall C by the NPS collaboration [37]. An additional element is a deflection magnet as discussed in Sec. 3 and below.

5.1 The Deflection Magnet

Our MC analysis (see Sec. 3) shows that for the WACS experiment the horizontal direction of the field is significantly better choice because of higher resolution for the out-of-plane correlation between a proton and an electron momenta. At large scattering angles, when the required solid angle of the photon arm is very large the calorimeter will be very close to the target (2.9 m) which results in the demanding of 0.6 Tm field integral in the magnet. Due to the considerations above we proposed to construct a deflection magnet as shown in Fig. 13. It has weight of 9.5 tons and require of 150 kW power. Due to significant width of the magnet (total of 100 cm with a 32 cm gap) the beam line will pass through the 16 cm tall cut in the yoke. Such a cut allow sufficient space for magnetic shielding of the beam line. Residual field integral on the beam line is of 100 G-meter.

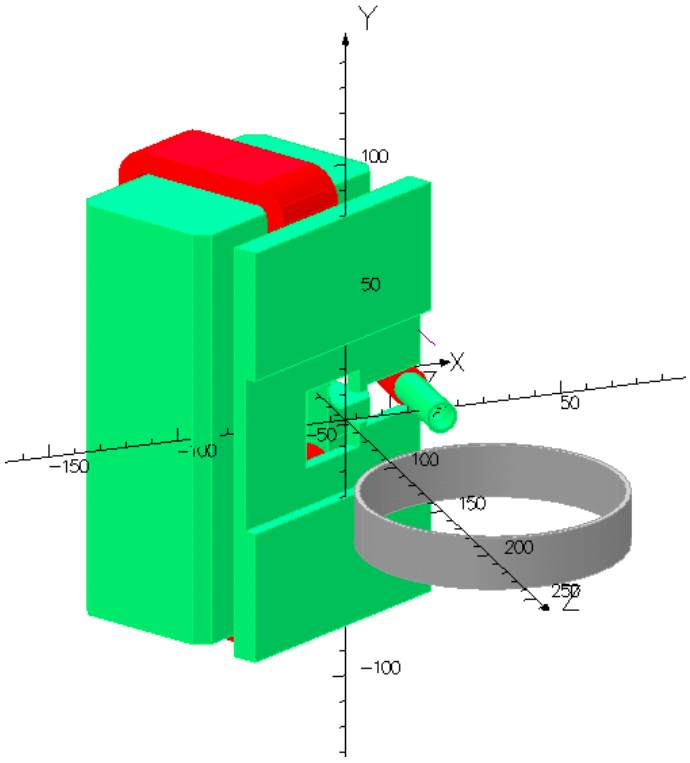

Figure 13: A picture of the deflection magent for the WACS experiment from the TOSCA analysis package. In this picture the magnet is placed at 30 degree scattering angle and 110 cm between the magnet center and the target.

6 Conclusions

We request 1000 hours of beamtime to measure the cross section with 10% accuracy (combined statistic and systematic) at s= 15.9 and 19.6 $(\mathrm{GeV}/c)^2$. This experiment will take place in Hall C, utilizing the HMS spectrometer to detect protons, and the Neutral Partical Spectrometer to detect scattered photons.

Knowledge of the cross ection in RCS at these kinematics will allow a rigirous test of the reaction mechanism for exclusive reactions at high s and t, which is crucial for the understanding of nucleon structure.

References

[1] N. Kivel and M. Vanderhaeghen, *JHEP* 1304 (2013) 029; arXiv:1212.0683.

[2] A.V. Radyushkin, *Phys. Rev.* **D 58**, 114008 (1998).

[3] M. Diehl, T. Feldmann, R. Jakob, P. Kroll, *Eur. Phys. J.* **C 8**, 409 (1999).

[4] H. W. Huang, P. Kroll, T. Morii, *Eur. Phys. J.* **C 23**, 301 (2002).

[5] M. Diehl and P. Kroll, arXiv:1302.4604.

[6] G. Eichmann and C. S. Fischer, *Phys. Rev.* **D 87** , 036006 (2013); arXiv:1212.1761.

[7] C. D. Roberts, *Prog. Part. Nucl. Phys.* 61, 50 (2008); I. C. Cloët, G. Eichmann, B. El-Bennich, T. Klahn, and C. D. Roberts, *Few Body Syst.* 46, 1 (2009).

[8] I. C. Cloë, C. D. Roberts, A. W. Thomas, arXiv:1304.0855.

[9] G. R. Farrar and H. Zhang, *Phys. Rev. Lett.* **41**, (1990) 1721, *Phys. Rev.* **D 65** (1990) 3348.

[10] A. S. Kronfeld and B. Nizic, *Phys. Rev.* **D 44**, 3445 (1991).

[11] M. Vanderhaeghen, P. A. M. Guichon and J. Van de Wiele, *Nucl. Phys.* **A 622**, 144c (1997).

[12] T. Brooks and L. Dixon, *Phys. Rev.* **D 62** 114021 (2000).

[13] R. Thomson, Alex Pang, and Cheng-Ryong Ji, *Phys. Rev.* **D 73** 054023 (2006).

[14] C. Hyde-Wright, A. Nathan, and B. Wojtsekhowski, spokespersons, JLab experiment E99-114.

[15] A. Danagoulian, V. H. Mamyan *et al.*, *Phys. Rev. Lett.* **98**, 152001 (2007).

[16] M. A. Shupe *et al.*, *Phys. Rev.* **D 19**, 1921 (1979).

[17] D. J. Hamilton, V. H. Mamyan *et al.*, *Phys. Rev. Lett.* **94**, 242001 (2005).

[18] M. Diehl *et al.*, *Phys. Rev.* **D 67**, 037502 (2003).

[19] G. A. Miller, *Phys. Rev.* **C 69**, 052201(R) (2004).

[20] F. Cano and J. M. Laget, *Phys. Lett.* **B 551**, 317 (2003).

[21] S. J. Brodsky and G. P. Lepage in *Perturbative Quantum Chromodynamics*, edited by A. Mueller (World Scientific, Singapore, 1989).

[22] S. J. Brodsky and G. Farrar, *Phys. Rev. Lett.* **31**, 1953 (1973).

[23] V. Matveev *et al.*, *Nuovo Cimento Lett.* **7**, 719 (1973).

[24] S. J. Brodsky and G. P. Lepage, *Phys. Rev.* **D 22**, 2157 (1980).

[25] M. Jones *et al.*, *Phys. Rev. Lett.* **84**, 1398 (2000).

[26] O. Gayou *et al.*, *Phys. Rev. Lett.* **88**, 092301 (2002).

[27] I. Pomerantz *et al.*, arXiv:1303.5049.

[28] F. Cano and J. M. Laget, Phys. Rev. D **65** (2002) 074022.

[29] X. Ji, *Phys. Rev.* **D 55**, 7114 (1997), *Phys. Rev. Lett.* **78**, 610 (1997).

[30] A.V. Radyushkin, *Phys. Lett.* **B 380**, 417 (1996), *Phys. Rev.* **D 56**, 5524 (1997).

[31] G. A. Miller and M. R. Frank, *Phys. Rev.* **C 65**, 065205 (2002)

[32] G. A. Miller, *Phys. Rev.* **C 66**, 032201 (2002)

[33] C. D. Roberts and A. G. Williams, Prog. Part. Nucl. Phys. **33**, 477 (1994).

[34] R. Gilman, A. Nathan, and B. Wojtsekhowski, spokespersons, JLab experiment E07-002.

[35] M. A. P. Carmignotto, *Neutral Particle Detector: Simulations*, Hall C Users Meeting, JLab, January 24, 2013.

[36] D. J. Hamilton et al., Nucl. Instr. Meth. A **643** (2011) 17. See also PhD thesis (in progress) of C. Fanelli (INFN-ISS).

[37] R. Ent, T. Horn, H. Mkrtchyan et al. (NPS Working Group), *Neutral-Pion Spectrometer Facility in Hall C*, Proposal to Jefferson Lab PAC40.

[38] M. Kubantsev et al., *Performance of the Primex Electromagnetic Calorimeter*, `arXiv:physics/0609201`, September 22, 2006; A. Gasparyan, *Performance of PWO crystal Detector for a High Resolution Hybrid Electromagnetic Calorimeter at Jefferson Lab*, Proceed. X Int. Conf. on Calorimetry in Particle Physics, Perugia, Italy, 29 March-2 April 2004, pp. 109-115.

[39] David J. Hamilton, *A simulation of the* 12 GeV *Hall C RCS experiment*, University of Glasgow, April 14, 2013 (unpublished).